A finite element model for convection-dominated melting and solidification problems

Zhen-Xiang Gong and Arun S. Mujumdar
Department of Chemical Engineering, McGill University, Montreal, Canada

Received February 1997
Accepted September 1997

Nomenclature

A	porosity function for the momentum equation
A^*	dimensionless form of A
A_{xy}	area of a computational domain
b	a small constant
c	specific heat
C	constant
f_H	enthalpy-temperature function
Fo	Fourier number
g_i	gravitational force vector
h	enthalpy
H	dimensionless enthalpy
k	heat conductivity
$\tilde{k}_i$	artificial diffusion coefficient
l	average element length
L_x	length of rectangular enclosure in x direction
L_y	length of rectangular enclosure in y direction
n_i	surface unit normal vector
p	fluid pressure
P	dimensionless fluid pressure
Pr	Prandtl number
q	heat flux
q_a	prescribed heat flux
q_c	convective heat flux
q_r	radiative heat flux
q_s	heat source
Q	instantaneous energy charged
Q_T	total energy charged
Q_M	maximum energy charged
Ra	Rayleigh number
s	boundary surface coordinate
Ste	Stefan number
t	time
T	temperature
T_0	reference temperature
T_m	melting point of PCM
T_w	isothermal wall temperature
u_i	velocity component
u_x	velocity in x direction
u_y	velocity in y direction
U	dimensionless velocity of x direction
V	dimensionless velocity of y direction
x,y	coordinate
X,Y	dimensionless coordinate

Greek symbols

α	diffusivity
β	expansion coefficient
θ	dimensionless temperature
Δh	latent heat
Δt	time step
λ	porosity of a mush zone
φ	shape function of velocity
$\tilde{\varphi}$	weighting function for momentum equation
ϑ	shape function of temperature
$\tilde{\vartheta}$	weighting function for energy equation
γ	penalty parameter
Γ	boundary
μ	viscosity
Ω	integration domain
ρ	density
ω	the angle horizontal direction to x axis
σ_{ij}	stress tensor

Superscripts

–	over bar, boundary value of the variable
0	initial value

Subscripts

l	liquid
n	nth time step
s	solid
x	component of x direction
y	component of y direction

International Journal of Numerical Methods for Heat & Fluid Flow
Vol. 8 No. 4, 1998, pp. 393–408.

1. Introduction

While a major effort has been devoted to the numerical solution of conduction-controlled phase change problems over the last three decades focus has shifted to convection-dominated problems only recently. Although the finite element method has been widely applied to solve conduction-controlled phase change problems, little effort has been made in the area of finite element solution of convection-dominated melting and solidification problems.

Gartling (1980) was the first to model convection-dominated melting and solidification problems with the standard Galerkin finite element technique. He employed the Boussinesq assumption and effective heat capacity method to solve the Navier-Stokes and energy equations. To account for the zero velocity condition as the liquid turns to solid or the solid becomes liquid he developed an approach which makes the viscosity a function of ΔH where ΔH is the cumulative energy of latent heat of a computational cell. When ΔH decreases from λ (where λ is the latent heat of the phase change) to 0 the value of viscosity increases to a large value thus simulating the liquid-solid phase change. Morgan (1981) presented an explicit finite element algorithm for the solution of convection-dominated melting and solidification problems. In his model he employed an enhanced heat capacity to treat the latent heat effect. To account for the velocity evolution at the phase change interface a simple approach was used which fixes the velocities to zero in a computational cell whenever the cumulative energy of latent heat of a cell reaches some predetermined value between 0 and λ. Usmani *et al.* (1992) reported an implicit finite element model based on effective heat capacity approach in combination with the standard Galerkin finite element method with a primitive variable formulation. They also employed the varying viscosity approach to model the velocity evolution at the phase change interface.

In the context of the finite volume method Voller and Prakash (1987) and Brent *et al.* (1988) investigated various ways of dealing with zero solid velocities in fixed grid enthalpy solutions of freezing in a thermal cavity. They assumed the mushy region to be a pseudo porous medium with the porosity decreasing from 1 to 0 as ΔH decreases from λ to 0. In this way, on prescribing a “Darcy” source term the velocity value arising from the solution of the momentum equations are inhibited, reaching values close to zero on complete solid formation. The enthalpy-porosity model has proved to be effective in solving both isothermal and nonisothermal phase change problems.

In this paper a streamline upwind/Petrov Galerkin finite element model in combination with primitive variables is presented for solving convection dominated melting and solidification problems. Boussinesq assumption is invoked and two-dimensionality is assumed. The enthalpy-porosity approach is utilized to model the velocity evolution at the phase change interface. Penalty formulation is employed to treat the incompressibility constraint in the momentum equations. Simulations are carried out for melting of a phase change material in a rectangular cavity heated from below.

2. Mathematical formulation

2.1 Governing equations

For the mathematical description of a melting or freezing process the following assumptions are made:

(1) heat transfer in the PCM is conduction/convection controlled, and the melt is Newtonian and incompressible;

(2) the flow in the melt is laminar and viscous dissipation is negligible;

(3) the densities of the solid and liquid are equal;

(4) the Boussinesq assumption is valid for free convection, i.e. density variations are considered only insofar as they contribute to buoyancy, but are otherwise neglected;

(5) the solid PCM is fixed to the container wall during the melting process.

Based on the above assumptions, the governing equations in tensor form are

Solid region:

$$\rho \frac{\partial h}{\partial t} = (k_s T_{,j})_{,j} + q_s \tag{1}$$

Liquid region:

Continuity equation

$$u_{i,i} = 0 \tag{2}$$

Momentum equation

$$\rho(\frac{\partial u_i}{\partial t} + u_j u_{i,j}) = -p_{,i} + [\mu(u_{i,j} + u_{j,i})]_{,j} - \rho g_i \beta (T - T_0) \tag{3}$$

Energy equation

$$\rho(\frac{\partial h}{\partial t} + u_j T_{,j}) = (k_l T_{,j})_{,j} + q_s \tag{4}$$

The initial and boundary conditions are

initial conditions

$$T(x,0) = T^0(x)$$
$$u_i(x,0) = u_i^0(x) \tag{5}$$

boundary conditions

$$u_i = \bar{u}_i(s,t) \qquad \text{on } \Gamma_u$$

$$t_i = \sigma_{ij} n_j(s) = \bar{t}_i(s,t) \qquad \text{on } \Gamma_t$$

$$T = \bar{T}(s,t) \qquad \text{on } \Gamma_T \tag{6}$$

$$q = -(kT_{,j})n_j(s) = q_a(s,t) + q_c(s) + q_r(s) \qquad \text{on } \Gamma_q$$

2.2 Enthalpy-porosity model

Two methods are available to account for the physics of the evolution of the flow at the solid/liquid phase change interface in fixed-grid methods. One is the enthalpy-porosity model (Brent *et al.*, 1988; Voller and Prakash, 1987); the other is the viscosity model (Gartling, 1980; Usmani *et al.*, 1992). The enthalpy-porosity is employed in this study.

The enthalpy-porosity model treats the mushy region as a porous medium. The flow in the mush is governed by Darcy's law. According to the enthalpy-porosity model (Brent *et al.*, 1988; Voller and Prakash, 1987) equations (1) through (4) can be rewritten as follows:

$$u_{i,i} = 0 \tag{7}$$

$$\rho\left(\frac{\partial u_i}{\partial t} + u_j u_{i,j}\right) = -p_{,i} + [\mu(u_{i,j} + u_{j,i})]_{,j} - \rho g_i \beta(T - T_0) + Au_i \tag{8}$$

$$\rho\left(\frac{\partial h}{\partial t} + u_j T_{,j}\right) = (kT_{,j})_{,j} + q_s \tag{9}$$

In equation (8)

$$A = -C(1-\lambda)^2 / (\lambda^3 + b) \tag{10}$$

in which b is a small constant introduced to avoid division by zero and C is a constant accounting for the morphology of the mushy region. In general b is assigned a value of 0.001. For isothermal phase change C is assigned a value of 1.6×10^6.

2.3 The penalty formulation

Two models can be used to treat the incompressibility constraint in the momentum equation. One is the penalty formulation (Brooks and Hughes, 1982; Hughes *et al.*, 1979) and the other is the so-called slightly compressible formulation (Brooks and Hughes, 1982; Dyne and Heinrich, 1993). In this study the penalty formulation is employed to treat the incompressibility constraint.

In the penalty formulation, the continuity equation is replaced by

$$u_{i,i} = -\frac{1}{\gamma} p \tag{11}$$

where γ is the penalty parameter which is generally assigned a value of 1.0×10^9.

As a result of the utilization of the penalty approximation, the pressure term and the mass conservation equation are eliminated from the system of equations (equations (7) through (9)). The governing equations (equations (7)-(9)) then become

$$\rho\left(\frac{\partial u_i}{\partial t} + u_j u_{i,j}\right) = \frac{1}{\gamma}(u_{i,i})_{,i} + [\mu(u_{i,j} + u_{j,i})]_{,j} - \rho g_i \beta(T - T_0) + Au_i \quad (12)$$

$$\rho\left(\frac{\partial h}{\partial t} + u_j T_{,j}\right) = (kT_{,j})_{,j} + q_s \quad (13)$$

Once the velocity and temperature fields are known, the pressure variable is calculated a posteriori if desired at any step by solving the Poisson equation (Heinrich and Yu, 1988)

$$-(p_{,j})_{,j} = \rho(u_j u_{i,j})_{,i} + \rho\beta(g_j T_{,j}) \quad (14)$$

subject to homogeneous Neumann conditions along the boundary Γ; i.e.

$$n_j p_{,j} = 0 \quad (15)$$

In order to obtain a unique pressure field it is necessary to set the pressure at one point in the domain equal to a reference pressure.

3. Finite element model

Following the work of Brooks and Hughes (1982) and Argyris (1992) the streamline upwind/Petrov-Galerkin method is applied to the convection and source terms of the momentum and energy equations. After spacewise discretization of equations (12) and (13) in two dimensions subject to above mentioned boundary conditions we obtain the following semi-discrete equation:

$$\begin{bmatrix} M & 0 & 0 \\ 0 & M & 0 \\ 0 & 0 & N \end{bmatrix} \begin{Bmatrix} \dot{u}_x \\ \dot{u}_y \\ \dot{T} \end{Bmatrix} + \begin{bmatrix} K_{11}+K_{22} & K_{12} & B_1 \\ K_{21} & K_{11}+K_{22} & B_2 \\ 0 & 0 & L_{11}+L_{22} \end{bmatrix} \begin{Bmatrix} u_x \\ u_y \\ T \end{Bmatrix} +$$

$$\begin{bmatrix} A_1(u)+A_2(v) & 0 & 0 \\ 0 & A_1(u)+A_2(v) & 0 \\ 0 & 0 & D_1(u)+D_2(v) \end{bmatrix} \begin{Bmatrix} u_x \\ u_y \\ T \end{Bmatrix} + \begin{bmatrix} P_{11} & P_{12} & 0 \\ P_{21} & P_{22} & 0 \\ 0 & 0 & 0 \end{bmatrix} \begin{Bmatrix} u_x \\ u_y \\ T \end{Bmatrix} +$$

$$\begin{bmatrix} A & 0 & 0 \\ 0 & A & 0 \\ 0 & 0 & 0 \end{bmatrix} \begin{Bmatrix} u_x \\ u_y \\ T \end{Bmatrix} = \begin{Bmatrix} F_1 \\ F_2 \\ G \end{Bmatrix} \quad (16)$$

Typical elements in these matrices are

$$M = \int_{\Omega} \rho \varphi \varphi^{T} \, d\Omega \tag{17}$$

$$N = \int_{\Omega} \rho c_{l} \, \vartheta \vartheta^{\mathrm{T}} d\Omega \tag{18}$$

$$K_{ij} = \int_{\Omega} \mu \frac{\partial \varphi}{\partial x_i} \frac{\partial \varphi}{\partial x_j} d\Omega \tag{19}$$

$$L_{ij} = \int_{\Omega} k \frac{\partial \vartheta}{\partial x_i} \frac{\partial \vartheta}{\partial x_j} d\Omega \tag{20}$$

$$A_i(U_j) = \int_{\Omega} \rho \tilde{\varphi} u_j \frac{\partial \varphi}{\partial x_i} d\Omega \tag{21}$$

$$D_i(U_j) = \int_{\Omega} \rho c_l \, \tilde{\vartheta} u_j \frac{\partial \vartheta}{\partial x_i} d\Omega \tag{22}$$

$$P_{ij} = \int_{\Omega} \frac{1}{\gamma} \frac{\partial \varphi}{\partial x_i} \frac{\partial \varphi}{\partial x_j} d\Omega \tag{23}$$

$$B_i = \int_{\Omega} \rho g_i \beta \varphi \vartheta^{T} d\Omega \tag{24}$$

$$F_i = \int_{\Gamma} \bar{t} \, \varphi \, d\Gamma + \int_{\Omega} \rho g_i \beta T_0 \varphi \, d\Omega \tag{25}$$

$$G = \int_{\Gamma} (q_a + q_c + q_r) \vartheta \, d\Gamma + \int_{\Omega} q_s \vartheta \, d\Omega \tag{26}$$

in which

$$\tilde{\varphi} = \varphi + \tilde{k}_1 u_j \varphi_{,j} \tag{27}$$

$$\tilde{\vartheta} = \vartheta + \tilde{k}_2 u_j \vartheta_{,j} \tag{28}$$

Following Heinrich and Yu (1988)

$$\tilde{k}_i = \frac{\xi_i l}{2\|u\|} \tag{29}$$

in which $\|u\|$ is the magnitude of the local velocity $\boldsymbol{u}$,

$$\|u\|^2 = u_i u_i \qquad \text{(sum)} \tag{30}$$

and l is an average element length whose definition is given in (Heinrich and Yu, 1988). The parameters ξ_i are given by

$$\xi_i = \coth \zeta_i - \frac{1}{\zeta_i} \tag{31}$$

$$\zeta_1 = \frac{\|u\| l}{2\mu / \rho} \tag{32}$$

$$\zeta_2 = \mathbf{Pr}\,\zeta_1 \tag{33}$$

It should be noted that the numerical integration of the pressure term (equation (23)) must be one order lower than that of the velocity terms. In this work, bilinear quadrilateral elements are used to perform all computations. A source-based scheme (Swaminathan and Voller, 1993; Voller, 1990) is used to treat the phase change effects. A backward Euler scheme is employed to accomplish the time discretization of equation (16).

5. Dimensionless form of the governing equations in two-dimensions

For convection-dominated two-dimensional melting or freezing problems subjected to the Dirichlet boundary condition (first kind boundary condition) the dimensionless governing equations are:

Solid region:

$$\frac{\partial H}{\partial Fo} = \frac{k_s}{k_l} Ste\left(\frac{\partial^2\theta}{\partial X^2} + \frac{\partial^2\theta}{\partial Y^2}\right) \tag{34}$$

Liquid region:

$$\frac{\partial U}{\partial X} + \frac{\partial V}{\partial Y} = 0 \tag{35}$$

$$\frac{\partial U}{\partial Fo} + U\frac{\partial U}{\partial X} + V\frac{\partial U}{\partial Y} = -\frac{\partial P}{\partial X} + \mathbf{Pr}\left(\frac{\partial^2 U}{\partial X^2} + \frac{\partial^2 U}{\partial Y^2}\right) + Ra\,\mathrm{Pr}\sin\omega + A^{*}U \tag{36}$$

$$\frac{\partial V}{\partial Fo} + U\frac{\partial V}{\partial X} + V\frac{\partial V}{\partial Y} = -\frac{\partial P}{\partial Y} + \mathbf{Pr}\left(\frac{\partial^2 V}{\partial X^2} + \frac{\partial^2 V}{\partial Y^2}\right) + Ra\,\mathrm{Pr}\cos\omega + A^{*}V \tag{37}$$

$$\frac{\partial H}{\partial Fo} + U\frac{\partial H}{\partial X} + V\frac{\partial H}{\partial Y} = Ste\left(\frac{\partial^2\theta}{\partial X^2} + \frac{\partial^2\theta}{\partial Y^2}\right) \tag{38}$$

in which

$$\begin{cases} H = \dfrac{c_s}{c_l} Ste\theta, & \theta < 0 \\ H = Ste\theta + 1 & \theta > 0 \end{cases} \tag{39}$$

and

$$U = \frac{u_x L_y}{\alpha_l}, \quad V = \frac{u_y L_y}{\alpha_l}, \quad \theta = \frac{T - T_m}{T_w - T_m}, \quad H = \frac{h - c_s T_m}{\Delta h}, \quad P = \frac{p L_y^2}{\rho \alpha_l^2},$$

$$X = \frac{x}{L_y}, \quad Y = \frac{y}{L_y}, \quad A^* = \frac{A L_y^2}{\rho \alpha_l}, \quad Fo = \frac{t \alpha_l}{L_y^2}, \quad \mathrm{Pr} = \frac{c_l \mu}{k_l}, \tag{40}$$

$$Ra = \frac{\rho^2 c_l g \beta L_y^3 (T_w - T_m)}{\mu k_l}, \quad Ste = \frac{c_l (T_w - T_m)}{\Delta h}$$

It is clear that melting and freezing phase change heat transfer including free convection is determined by the following five dimensionless parameters, Rayleigh number (*Ra*), Prandtl number (*Pr*), Stefan number (*Ste*), the ratio of solid/liquid specific heat (c_s/c_l), as well as the ratio of solid/liquid heat conductivity (k_s/k_l).

6. Test of the numerical model

The above-mentioned numerical model is verified by comparison with the experimental results of Gau and Viskanta (1986) and the implicit finite difference results of Lacroix (1992) for the melting of a pure metal (gallium) inside a two-dimensional rectangular cavity (height L_y = 0.0445m; width L_x = 0.089m). The gallium is assumed to be initially at its fusion temperature. The top and bottom boundaries are adiabatic. At time t = 0, the temperature of the left vertical wall is suddenly raised to a prescribed temperature above the melting point. The values of the governing dimensionless numbers and aspect ratio are listed in Table I for the test problem.

Figure 1 compares the predicted phase front with both the experimental results of Gau and Viskanta (1986) and the finite difference prediction of Lacroix (1992). It is seen from this figure that the present model is in good agreement with the results of the above-mentioned references. Experimental uncertainty values are not available.

The discrepancy between the predicted phase front of the present model and the experimental results is due to two possible reasons. First, in the experiment, the solid showed an initial subcooling of approximately 2°C. This degree of subcooling is significant in the light of the fact the heated wall was at only 8°C higher than the melting temperature of gallium. The second reason is that it is difficult to impulsively heat the vertical wall to a desired temperature in reality

Table I. Parameters used in the accuracy test runs

R	Aspect ratio L_y/L_x	0.5
Ra	Rayleigh number	2.2×10^5
Pr	Prandtl number	0.021
Ste	Stefan Number	0.042
c_s/c_l	Ratio of solid/liquid specific heat	1
k_s/k_l	Ratio of solid/liquid heat conductivity	1

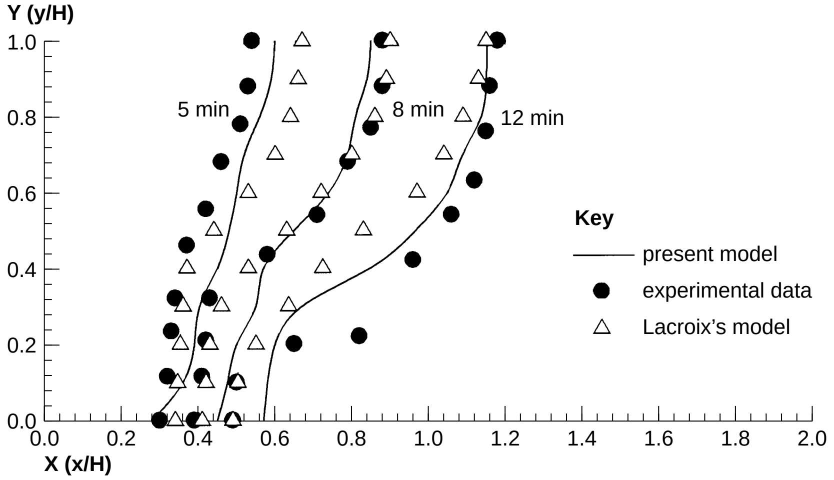

Figure 1. Comparison of the predicted phase front with experimental data

due to its finite thermal inertia. The discrepancy of predicted phase front between the present model and Lacroix's model is due to the difference of the numerical methods used. Lacroix used a front-tracking method while this model uses a fixed-grid enthalpy-porosity approach to model the phase change effects.

7. Results and discussions

Using the above-described numerical model simulation runs were carried out for melting of a PCM in a rectangular cavity heated from below. The side walls as well as the top wall are assumed to be adiabatic. The parameters for the computed problem are listed in Table II. The phase change material used is *n*-octadecane (99 per cent pure).

Grid-dependence experiments indicated that the maximum difference in the computed dimensionless cumulative energy charged, Q_T/Q_M, is within 3.6 per cent between using 20×20 elements with a dimensionless time step of 4.32×10^{-5} and 30×30 elements with the same time step; while the difference is only 1.5 per cent between using 30×30 elements with a dimensionless time step of 4.32×10^{-5} and 40×40 elements with a time step of 2.16×10^{-5}. Therefore, 30×30 elements with a time step of 4.32×10^{-5} were used for this and all the subsequent computations considering both accuracy and computing time.

R	Aspect ration L_y/L_x	1.0
Ra	Rayleigh number	2.844×10^6
Pr	Prandtl number	46.1
Ste	Stefan Number	0.138
c_s/c_l	Ratio of solid/liquid specific heat	0.964
k_s/k_l	Ratio of solid/liquid heat conductivity	2.419
θ_i	Initial dimensionless temperature	–0.0256

Table II. Parameters used in the simulation runs

It is known from experiments that three-dimensional convection cells develop and last for a short period of time during the early stage in a two-dimensional melting of a PCM heated from below (Benard, 1990; Hale and Viskanta, 1980). In this study we neglect three-dimensional convection since we employ a two-dimensional model. However, the duration of the three-dimensional convection is very short (Benard, 1990; Hale and Viskanta, 1980) compared with the whole melting process so that the two-dimensional results may be close to reality. No experimental data are available for direct validation at this time.

Figure 2 shows the predicted streamlines and isotherms at different Fo values for the computed problem ($Ra = 2.844 \times 10^6$). Figures 2-a1 through 2-a5 present the streamlines at Fo = 0.0864, 0.173, 0.259, 0.346 and 0.432, respectively, corresponding to Figures 2-a1 through 2-a5 Figures 2-b1 through 2-b5 display the isotherms. From Figures 2-a1 through 2-a5 it is seen that at Fo = 0.0864 a total of eight convection cells develop and these eight circulation cells result in a regular distribution of cusps on the liquid/solid phase change interface. The predicted phenomena are consistent with the published experimental results of Gau *et al.* (1983). With the increase of the melt depth the size of the convection cells increases and the number of the cells decreases. At Fo = 0.173 two main large circulation cells exist. With further increase of the melt depth the size of the left cell increases and that of the right cell decreases. Because of the asymmetric flow field the phase change interface is also asymmetric. The asymmetric flow patterns and phase change interface are in accord with the experimental results of Gau *et al.* (1983).

Corresponding to the flow patterns in Figures 2-a1 through 2-a5 Figures 3a and 3b present the local dimensionless heat flux distributions. According to the dimensionless energy equation (Equation (38)) the dimensionless heat flux is $\frac{\partial \theta}{\partial X}$. Figure 3a shows that the dimensionless heat flux distribution at Fo = 0.0864 is wave-like corresponding to the multiple convection cells of Figure 2-a1. There are four crests and three troughs in the dimensionless heat flux curve of Fo = 0.0864 displayed in Figure 3a. These crests and troughs correspond to the seven junctions of the eight convection cells in the streamlines in Figure 2-a1. The first crest from left corresponds to the junction of the first and second convection cells. The flow direction of the first circulation is clockwise and the second circulation is anti-clockwise. The liquid layers from the two circulation cells are cooled after passing the phase change interface and then reach the junction of the two circulation zones at the bottom. This causes a low temperature zone near the junction at the bottom surface of the container. The low temperature zone is seen in the isotherms in Figure 2-b1. Since the bottom surface of the container is isothermal, a low temperature near the bottom isothermal surface means a large temperature difference for heat transfer. This results in higher heat flux.

The first trough from left corresponds to the junction of the second and the third convection cells in Figure 2-a1, since the flow direction of the second circulation is anti-clockwise and the third circulation is clockwise. At the

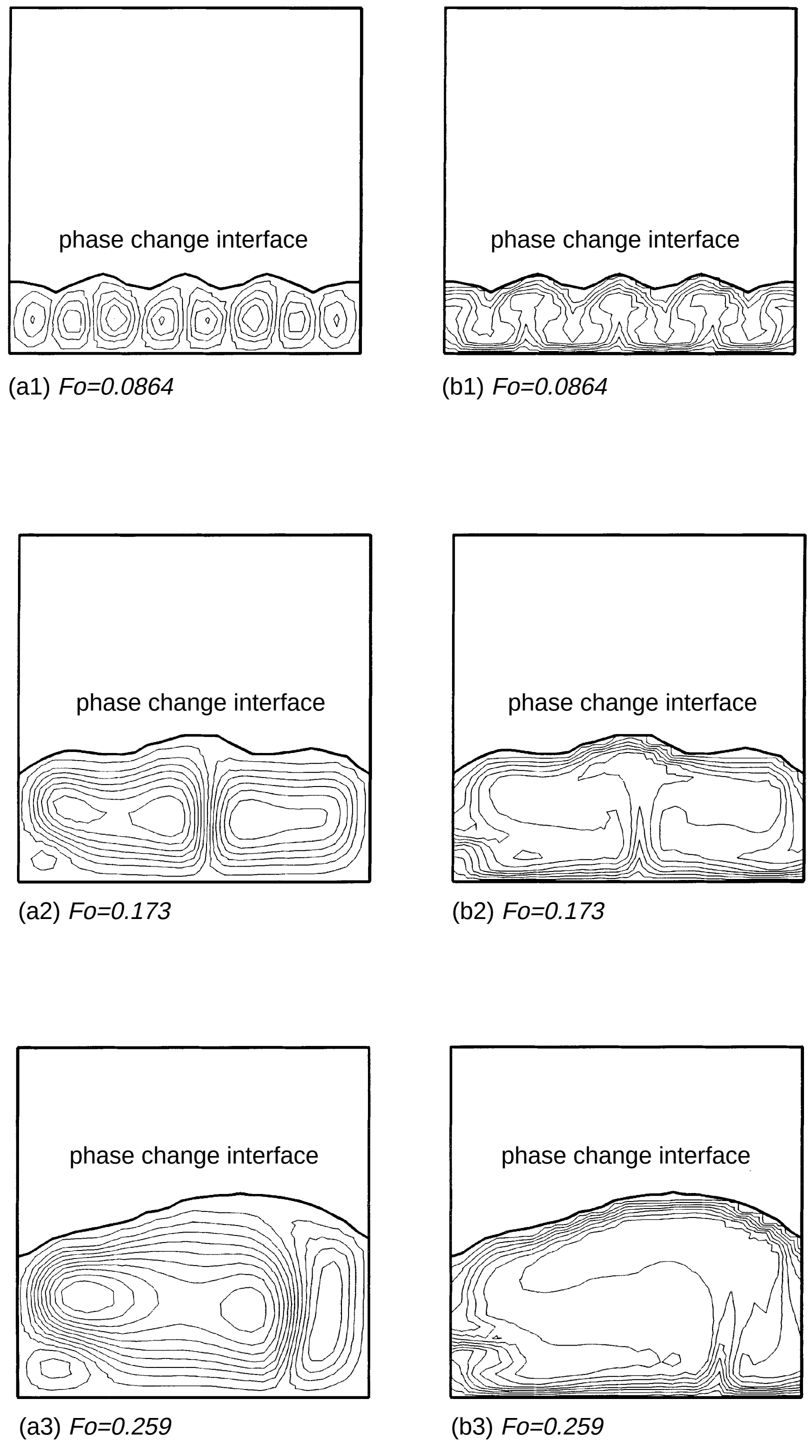
phase change interface
phase change interface
(a1) Fo=0.0864
(b1) Fo=0.0864
phase change interface
phase change interface
(a2) Fo=0.173
(b2) Fo=0.173
phase change interface
phase change interface
(a3) Fo=0.259
(b3) Fo=0.259

Figure 2.

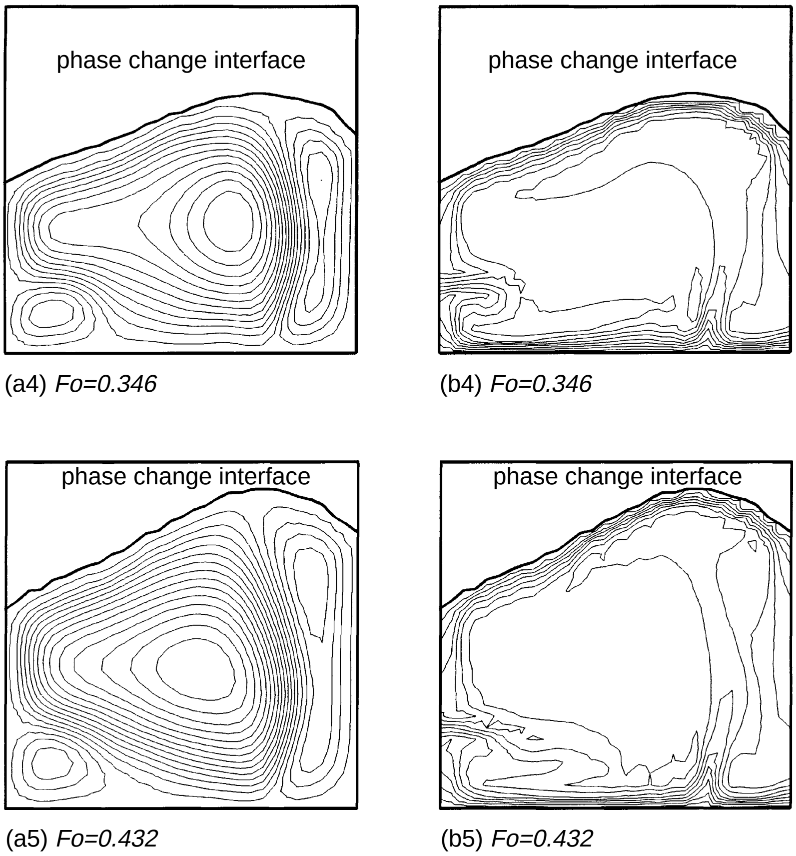

Figure 2.
Streamlines and isotherms in the melt zone for heating from below (Ra = 2.844 × 10^6)

junction of the two cells a high temperature zone is developed. This is shown in the corresponding isotherms in Figure 2-b1. A higher temperature near the bottom isothermal surface results in a lower temperature difference for heat transfer from the wall. The lower temperature difference results in reduced heat flux. Similar explanation applies to the other crests and troughs in the dimensionless heat flux distributions.

The heat flux distribution curve at Fo = 0.0173 in Figure 3a shows that the heat flux close to the left vertical wall is very low although the flow direction of the first large convection cell from left is anti-clockwise in Figure 2-a2. This is caused by the small circulation bubble in the bottom-left corner. This small circulation bubble results in a high temperature zone. The high temperature zone leads to a reduced heat flux along the bottom isothermal surface. Similarly, the trough on the heat flux curve corresponds to the junction of the two adjacent large convection cells seen in Figure 2-a2.

Figure 4 presents the predicted streamlines and isotherms at different *Fo* values for *Ra* = 5.688×10^6. Figures 4-a1 through 4-a4 show the streamlines at *Fo* = 0.0864, 0.173, 0.259 and 0.346, respectively. Corresponding to the flow fields of Figures 4-a1 through 4-a4 Figures 4-b1 through 4-b4 present the isotherms. From Figures 4-a1 through 4-a4 it is seen that during the early stage of the melting process the flow patters are similar to those obtained at the lower Rayleigh number of 2.844×10^6. With the growth of the melt depth the flow

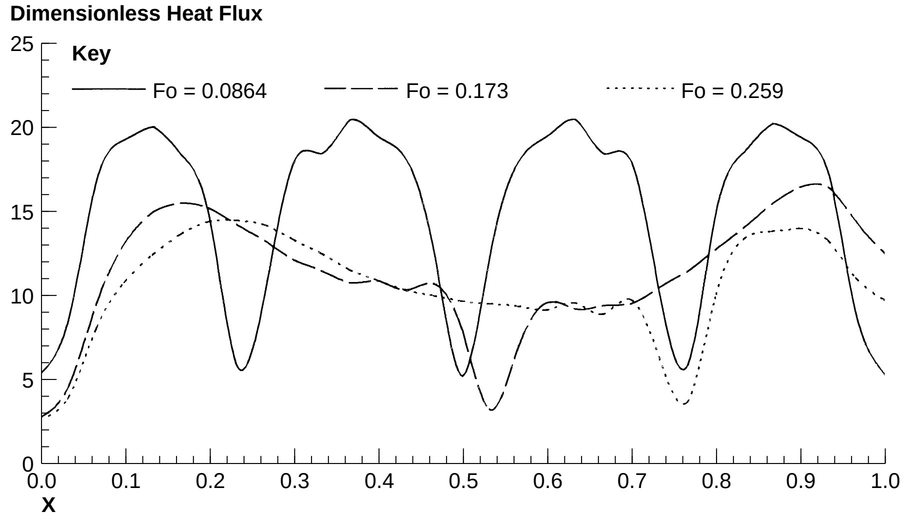

(a) *Fo = 0.0864, 0.173, 0.259*

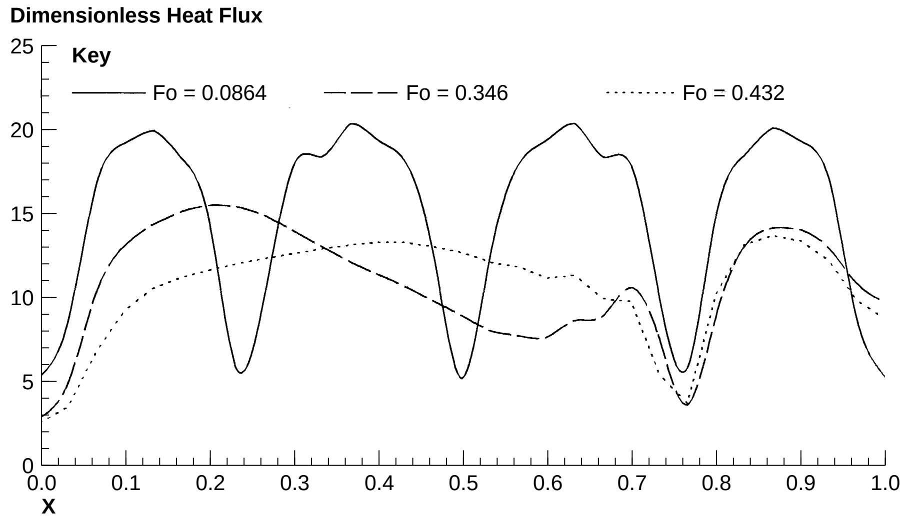

(b) *Fo = 0.0864, 0.346, 0.432*

Figure 3. Local dimensionless heat flux distribution along the heated surface at different Fo values (*Ra* = 2.844×10^6)

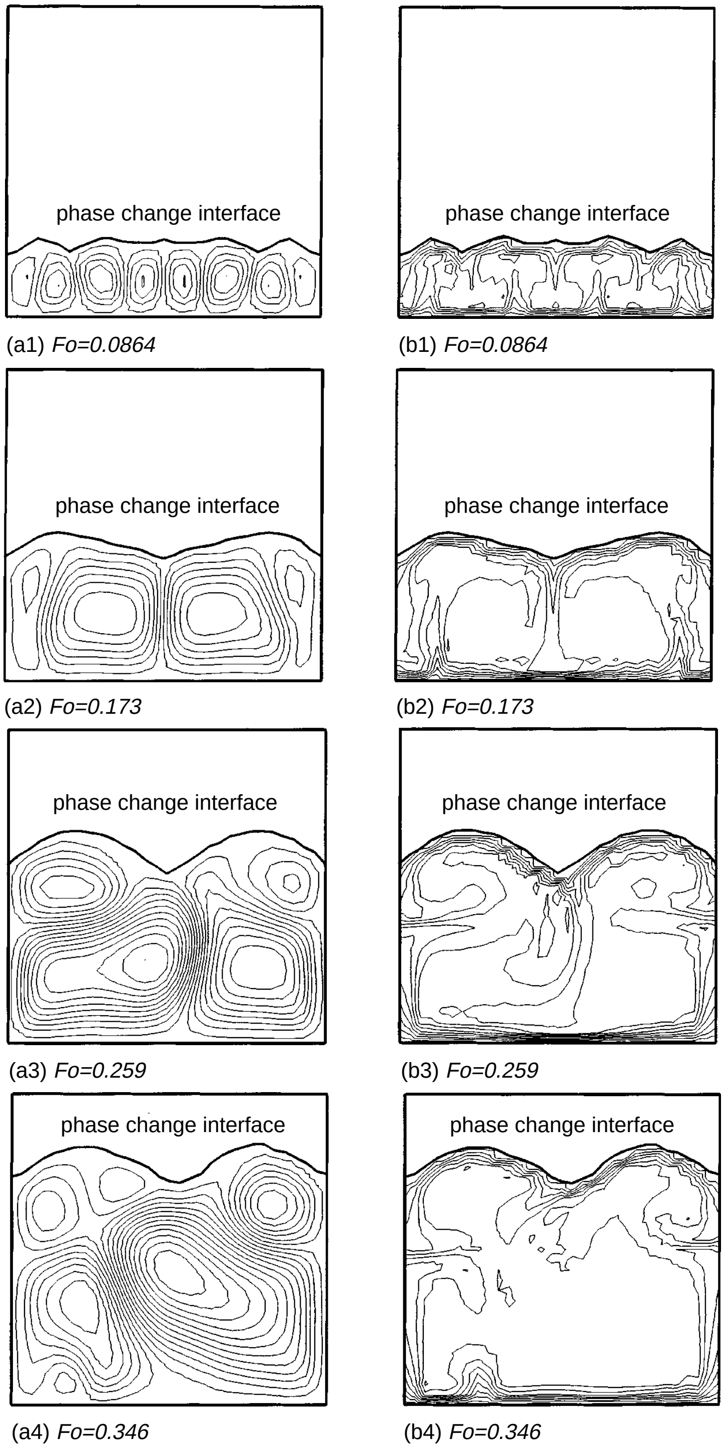

Figure 4.
Streamlines and isotherms in the melt zone for heating from below ($Ra = 5.688 \times 10^6$)

includes two large circulation cells and two small cells; the sizes and locations of both the large and small cells vary with time. It is interesting to note the Rayleigh number has a very significant effect on the flow patterns.

Corresponding to the flow patterns in Figures 4-a1 through 4-a4, Figure 5 shows the local dimensionless heat flux distribution curves for $Ra = 5.688 \times 10^6$ at different dimensionless times. It is seen in Figure 5 that the local dimensionless heat flux distributions are also very different from those in Figure 3. This is reflected in the difference in the flow patterns between these two cases.

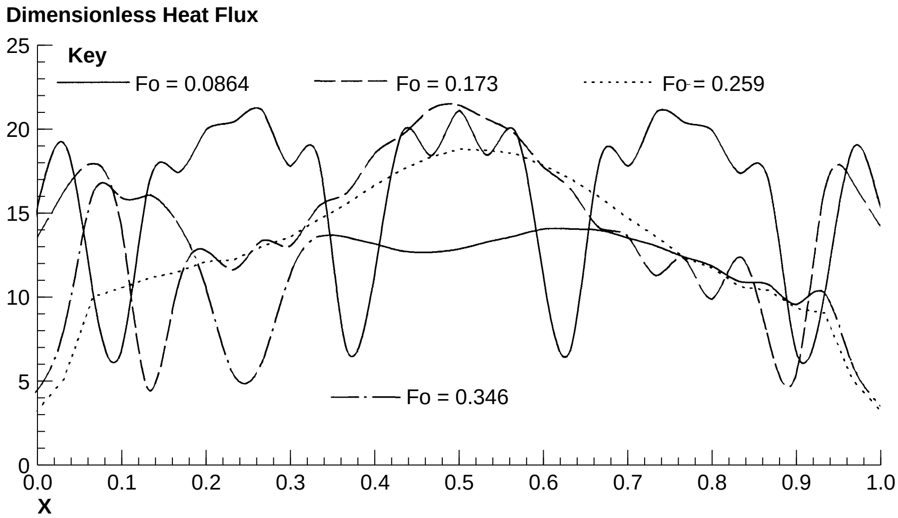

Figure 5. Local dimensionless heat flux distributions at the heated surface at different *Fo* values ($Ra = 5.688 \times 10^6$)

8. Concluding remarks

A finite element model was developed for the solution of two-dimensional melting and solidification problems. For the first time melting of a PCM in a rectangular cavity heated from below is simulated. Complex flow patterns are obtained which are qualitatively consistent with the published experimental results.

References

Argyris, J. (1992), "Petrov-Galerkin finite element approach to coupled heat and fluid flow", *Comp. Meth. Appl. Mech. Eng.,* Vol. 94, pp. 181-200.

Benard, H. (1990), "Tourbillions cellulaires dans une nappe liquide", *Revue Générale des Sciences Pures et Appliqées,* Vol. 11, pp. 1309-28, 1900.

Brent, A.D., Voller, V.R. and Reid, K.J. (1988), "Enthalpy-porosity technique for modelling convection-diffusion phase change: application to the melting of a pure metal", *Numerical Heat Transfer,* Vol. 13, pp. 297-318.

Brooks, A.N. and Hughes, T.J.R. (1982), "Streamline upwind/Petrov-Galerkin formulations for convection dominated flows with particular emphasis on the incompressible Navier-Stokes equations", *Comp. Meth. Appl. Mech. Eng.,* Vol. 32, pp. 199-259.

Dyne, B.R. and Heinrich, J.C. (1993), "Physically correct penalty-like formulations for accurate pressure calculation in finite element algorithms of the Navier-Stokes equations", *Int. J. Num. Meth. Eng.,* Vol. 36, pp. 3883-3902.

Gartling, D.K. (1980), "Finite element analysis of convective heat transfer problems with change of phase", in Morgan, K., Taylor, C. and Brebbia, C.A. (Eds), *Computer Methods in Fluids,* Pentech, London, pp. 257-84.

Gau, C. and Viskanta, R. (1986), "Melting and solidification of a pure metal on a vertical wall", *J. Heat Transfer,* Vol. 174, pp. 174-81.

Gau, C., Viskanta, R. and Ho, C.J. (1983), "Flow visualization during solid-liquid phase change heat transfer II. Melting in a rectangular cavity", *Int. Comm. Heat Mass Transfer,* Vol. 10, pp. 183-90.

Hale, N.W., Viskanta, R. (1980), "Solid-liquid phase change heat transfer and interface motion in materials cooled or heated from above or below", *Int., J. Heat Mass Transfer,* Vol. 23, pp. 283-92.

Heinrich, J.C. and Yu, C.C. (1988), "Finite element simulation of buoyancy-driven flows with emphasis on natural convection in a horizontal circular cylinder", *Comp. Meth. Appl. Mech. Eng.,* Vol. 69, pp. 1-27.

Hughes, T.J.R., Liu, W.K. and Brooks, A. (1979), "Review of finite element analysis of incompressible viscous flows by the penalty function formulation", *Journal of Computational Physics,* Vol. 30, pp. 1-60.

Lacroix, M. (1992), "Predictions of natural-convection-dominated phase-change problems by the vorticity-velocity formulation of the Navier-Stokes equations", *Numerical Heat Transfer, Part B,* Vol. 22, pp. 79-93.

Morgan, K. (1981), "Numerical analysis of freezing and melting with convection", *Comp. Meth. Appl. Mech. Eng.,* Vol. 28, pp. 275-84.

Swaminathan, C.R. and Voller, V.R. (1993), "On the enthalpy method", *Int. Num. Meth. Heat Fluid Flow,* Vol. 3, pp. 233-44.

Usmani, A.S., Lewis, R.W. and Seetharamu, K.N. (1992), "Finite element modeling of natural-convection-controlled change of phase", *Int. J. Num. Meth. Eng.,* Vol. 14, pp. 1019-36.

Voller, V.R. (1990), "Fast implicit finite-difference method for the analysis of phase change problems", *Num. Heat Transfer,* Vol. 17, pp. 155-69.

Voller, V.R. and Prakash, C. (1987), "A fixed grid numerical modelling methodology for convection-diffusion mushy region phase-change problems", *Int. J. Heat Mass Transfer,* Vol. 30, pp. 1709-19.